Check for updates

The Numerical Approach to Mosaic Patterns in Filament-Wound Composite Pipes

Paweł Stabla[1] · Michał Smolnicki[1] · Wojciech Błażejewski[1]

Abstract
This paper is focused on radial-compression of filament-wound composite pipes. An important but frequently disregarded is the issue of the choice of the winding pattern. The influence of the pattern on the strength of pipes is the subject of the investigation. Since the real geometry of filament-wound tubes is complicated researchers use simplified models (especially in "zig-zag" area), which are insufficient to reflect real behavior of tubes. An attempt to investigate a more precise geometry is presented in this work. A python script is used to model the particular areas typical for filament-wound elements. Hashin criterion is used to reflect damage in the material during compression. Results of numerical simulations are discussed and compared with experimental from other researchers. Based on the prepared model – the influence of pattern on the strength of a composite pipe is possible. Although some improvements may be introduced, a satisfactory agreement between the experiment and numerical simulation was achieved.

1 Introduction

Filament Winding (FW) is believed to be the most suitable and efficient technology to manufacture composite axisymmetric parts, such as pressure vessels, tubes, pipes [1-3] The process characterize a continuous fiber deposition onto a mandrel which provides good strength properties of the element. In wet winding, thanks to the impregnation system, the fiber tow is sufficiently saturated, and the final product includes fewer air voids [4].

Since filament winding is mainly used for manufacturing axisymmetric products, there are a lot of scientific interests concentered mainly on composite pressure vessels and pipes. The main tests being conducted on filament-wound elements are internal pressure loading

✉ Paweł Stabla
pawel.stabla@pwr.edu.pl

Michał Smolnicki
michal.smolnicki@pwr.edu.pl

1   Department of Mechanics, Materials and Biomedical Engineering, Wroclaw University of Science and Technology, Wroclaw, Poland

[5-8] external pressure loading [9, 10], axial compression [11, 12], radial compression [13], torsion test [14, 15] and split-disc method [16, 17]. Moreover, filament-wound elements find a great application possibilities in civil engineering such as tubes filled with concrete [18-21], where a great improvement of the mechanical behavior was observed after implementing the GFRP reinforcement.

Eggers et al. [22] evaluated the influence of the winding angle, stacking sequence and diameter-to-thickness ratio on the mechanical response of composite rings under various loading. The investigation revealed that for radial compression, axial compression and hoop tensile loading the dominant failure modes were, respectively, delamination, delamination and minor off-axis cracks, and fiber/matrix debonding and fiber breakage. Zu et al. [23] worked on the non-geodesic trajectories in the manufacturing of composite pressure vessels and found a satisfactory agreement between the numerical and experimental studies. Almeida Jr et al. [24] implemented the genetic algorithm to obtain the optimal stacking sequence of the filament-wound pipe under internal pressure, but without the consideration of winding pattern. A damage model to predict the response of filament wound tubes under external pressure and radial compression was developed [10, 13]. There was a good agreement between experiment and numerical results found.

The pattern issue is not widely discussed in the literature regarding the filament-wound pipes. One of the first mentions is reported by Rousseau et al. [25], who performed a set of pressure tests on the glass/epoxy tubes of ±55°. They concluded, that the increase of the degree of interweaving (the higher pattern number) influence the damage growth, but only for closed-ended internal-pressure loading and weeping test. In the case of the tensile test and pure internal pressure, no significant impact of the pattern was revealed. Morozov [26] conducted numerical research in the field of filament-wound pipes with different patterns under internal pressure loading. He concluded that the conventional mechanical approach, where the pattern influence on the geometry is not taken into account, may underestimate the stress distribution in shells. Another research [27] investigated the influence of winding pattern (1/1, 3/1 and 5/1) on filament wound composite cylinders under axial compression under hydrothermal conditioning. The best performance for both axial compressive strength and stiffness was established for 3/1 winding pattern, irrespective of the environmental conditioning. The high number of interweaving areas slightly decreased the local buckling and postponed crack propagation after the local buckling occurred. Shen et al. [11, 28] introduced a novel method for calculating the stiffness of the filament-wound tubes. A 3-step analysis was performed to alert the ABD matrix depending on the fiber undulations and crossovers. There was also implemented of an approach distinguishing the laminate region and the undulation region in numerical analysis using the macro and mesoscopic method. The uneven strain distribution occurred in the specimen, which influenced the failure of the composite.

Judging from the literature analysis, the great effort was put in the numerical investigation of filament-would composite structures. Nevertheless, the pattern issue and its influence on the final composite layup was insufficiently investigated. Some researchers examined the specimens with the respect to pattern number, but used a simplification in terms of the interweaving areas. This article attempts to bridge the literature gap in the field of numerical investigation of "zig-zag" area in filament-wound composite structures.

2 Theoretical Background

In FW parts, pattern geometry is an inevitable feature of the technology. The pattern is generated due to the cyclic deposition of the tow onto the mandrel. It is described by an integer number that reflects the number of diamond-shaped regions on the circumference of the mandrel. Each of the diamond consist of the two triangle areas with the laminate of -α/+α and +α/-α. Between those triangles, there is the so-called "zig-zag" area, where the interweavings occur [29]. Therefore, depending on the pattern number (the number of diamonds on the circumference), the amount of the discontinuity varies significantly. Moreover, for the same winding angle and mandrel diameter, different winding patterns may result in a different degree of coverage. The exemplary pattern is presented in Fig. 1.

The mechanism of interlaces creation is presented in Fig. 2.

In the numerical model, Hashin failure criteria are used to identify the status of the stress component at which failure happens [30]:

$$\left(\frac{\sigma_{11}}{X^T}\right)^2 + \alpha\left(\frac{\tau_{12}}{S^L}\right)^2 \geq 1 \sigma_{11} \geq 0 \text{ fibre tension} \tag{1}$$

$$\left(\frac{\sigma_{11}}{X^C}\right)^2 \geq 1 \sigma_{11} \leq 0 \text{ fibre compression} \tag{2}$$

$$\left(\frac{\sigma_{22}}{Y^T}\right)^2 + \left(\frac{\tau_{12}}{S^L}\right)^2 \geq 1 \sigma_{22} \geq 0 \text{ matrix tension} \tag{3}$$

$$\left(\frac{\sigma_{22}}{2S^T}\right)^2 + \left(\left(\frac{Y^C}{2S^T}\right)^2 - 1\right) \cdot \frac{\sigma_{22}}{Y_C} + \left(\frac{\tau_{12}}{S^L}\right)^2 \geq 1 \sigma_{22} \leq 0 \text{ matrix compression} \tag{4}$$

where σ_{11}, σ_{22} and τ_{12} denotes longitudinal, transverse and in-plane shear stress components. X^T, X^C, Y^T, Y^C, S^T and S^L stand for longitudinal tensile, longitudinal compressive, transverse tensile, transverse compressive and in-plane longitudinal and transverse shear strength components. These criteria are able to distinguish four damage mechanisms: fibre tension, fibre compression, matrix tension and matrix compression.

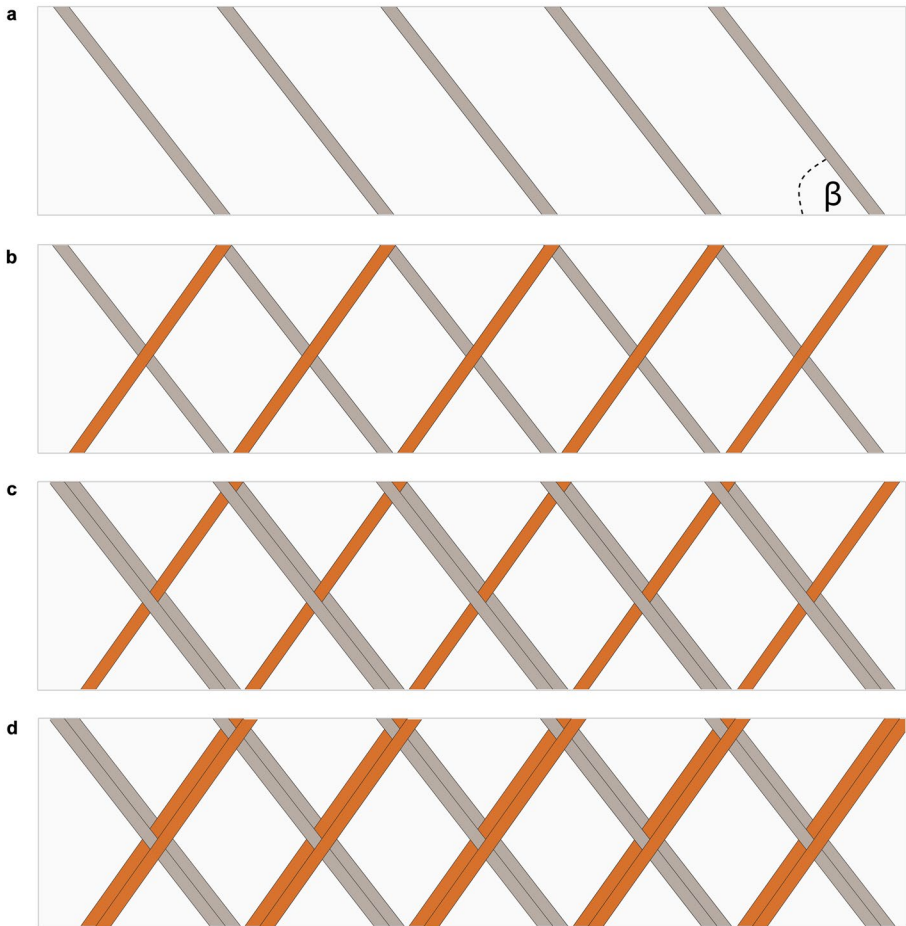Fig. 1 Wound laminate structure pattern 2/1 with 18 bands
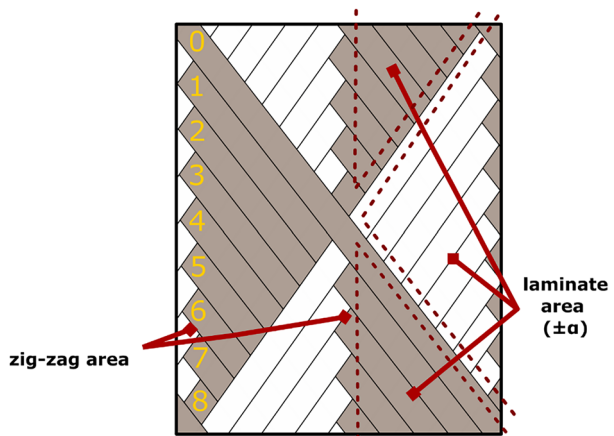
Fig. 2 Mechanism of interlaces formation

The α coefficient indicates the contribution of the shear stress to the fibre tensile initiation criterion. Depending on the value of the coefficient, the failure criteria can be set to obtain the model of Hashin and Rotem [31] for $\alpha = 0$ or the model of Hashin where $\alpha = 1$.

The outcome of damage is taken into consideration by the stiffness coefficients reduction as follows:

$$\sigma = C : \varepsilon \tag{5}$$

Where: represents a tensor double contraction and C matrix is the damaged stiffness given matrix by:

$$C = \begin{bmatrix} (1 - d_f)E_1/\Delta & (1 - d_f)(1 - d_m)v_{21}E_1/\Delta & 0 \\ (1 - d_f)(1 - d_m)v_{12}E_2/\Delta & (1 - d_m)E_2/\Delta & 0 \\ 0 & 0 & (1 - d_s)G_{12} \end{bmatrix} \tag{6}$$

$$\Delta = 1 - \left(1 - d_f\right)\left(1 - d_m\right)v_{12}v_{21} \tag{7}$$

$$d_s = 1 - (1 - d_f^t)(1 - d_f^c)(1 - d_m^t)(1 - d_m^c) \tag{8}$$

where ε is the strain, σ is the apparent stress, E_1, E_2 are the fibre direction and perpendicular to the fibre moduli, G_{12} refers to in-plane shear modulus, $v_{12}v_{21}$ are the in-plane Poisson's ratios, and $d_f^t, d_f^c, d_m^t, d_m^c$, are damage variables for fibre and matrix in tension and compression. Noticeably, the shear damage variable is not an independent value but is described in terms of the remaining damage variables.

The $d_f^t, d_f^c, d_m^t, d_m^c$, that describe the fibre and matrix damage in tension and compression refers to the four damage initiation modes Eqs. 1, 2, 3 and 4. Since each material point is either in tension or compression, the four damage variables may reduce to two variables as follows:

$$d_f = \begin{cases} d_f^t \text{if} \sigma_{11} \geq 0 \\ d_f^c \text{if} \sigma_{11} < 0 \end{cases} \tag{9}$$

$$d_m = \begin{cases} d_m^t \text{if} \sigma_{22} \geq 0 \\ d_m^c \text{if} \sigma_{22} < 0 \end{cases} \tag{10}$$

Effective stress (11) must be introduced instead of nominal stress to enable usage of the damage evolution criteria. The same Eqs. 1, 2, 3, and 4 are used in the criteria. The effective stress is described as:

$$\sigma' = M^{-1} : \sigma \tag{11}$$

Where M is the damage operator:

$$M = \begin{bmatrix} \frac{1}{(1-d_f)} & 0 & 0 \\ 0 & \frac{1}{(1-d_m)} & 0 \\ 0 & 0 & \frac{1}{(1-d_s)} \end{bmatrix} \tag{12}$$

Before the damage initiation happens, the M operator is equal to identify matrix and $\sigma' = \sigma$. When damage initiation and evolution occur for at least one mode, the damage operator becomes significant in the criteria for damage initiation of other modes [32, 33].

In the context of patterns in filament-wound cylinders, the aim of this work is to investigate the importance of the novel approach to 'zig-zag' area modelling with the use of finite element method. A described in the next chapter script is used to generate the characteristic area and the non-linear analysis of radial compression is performed. The numerical predictions are compared with experimental results obtained by of Lisôba et al. [34]. The aim of this paper is to describe a more precise way of carrying out numerical simulations of compressed winded tubes or vessels.

3 Wound Pipes Properties Determination

The geometry of wound pipes is quite complicated. Preparation of geometric model request line projection on the cylindrical surfaces. The more bands are used, the more projections are needed. The number of used bands for one pipe can vary from few to

several dozens. This is the reason why researchers used to simplify models which split the surface of the pipe to triangles or even just consider plain tube with lamina material assigned. These approaches do not take into account the zig-zag area, which leads to some discrepancy with fabricated pipes. However, by using scripting, it is possible to generate a precise model in which the material can be independently assigned to every single diamond. This is a more realistic approach – exemplary triangle used in past research is shown with the new precise assigning method in Fig. 3.

In the purpose of checking the influence of different parameters on the strength of wound pipes, python script for Abaqus was prepared. Using python scripting language one can replace whole pre-processing traditionally made in Abaqus-CAE (with GUI). Thus it is possible to automatize the entire process of simulation and consider a large group of different input parameters. The workflow of this script is presented in Fig. 4.

The geometry of bands is created using line projection on the cylindrical surface of the pipe. First datum points are created based on winding angle and number of bands. Then imaginary segment between each pair of consecutive points from the same band is projected on the surface and used as a partition tool. The idea of this operation is simple but even for reasonably small models, i.e. 100 mm length pipe with 24 bands and winding angle 60° number of such operations is above 3000. The result of this process is presented in Fig. 5 the cylindrical surface is split into diamonds.

After a geometrical model is finished, the material is assigned in such a manner that stacking sequence in every single diamond corresponds with reality. This means that there is a need to investigate how the material is oriented in the lower and upper layer. In Fig. 6 (left) half of the winding cycle can be observed– i.e. band is wound from one side to another. In the right picture, there is a whole single cycle i.e. the band is wound from one side to another and back again – one cycle of the layer. This is the reason for forming diamonds in a prepared model.

Depending on a different pattern i.e. an order in which subsequent bands are wound) material should be assigned in various ways. Exemplary patterns are presented in Fig. 7 in the left there is a 2/1 pattern and in the right there is 7/1 pattern for the tube with 50.4 mm diameters and 100 mm length.

The material is defined as a composite layup, which allows assigning a few layers of materials, which can be oriented independently of each other. Both layers are defined using lamina material type – what allows to define Young Modulus in fibre direction and perpendicular to them, Poisson's coefficient and Kirchhoff Modulus in all three directions. Typically used in this research ply stack sequence and orientations is presented in Fig. 8.

Fig. 3 Possible simplification of material assignation (right) and zig-zag area (left)
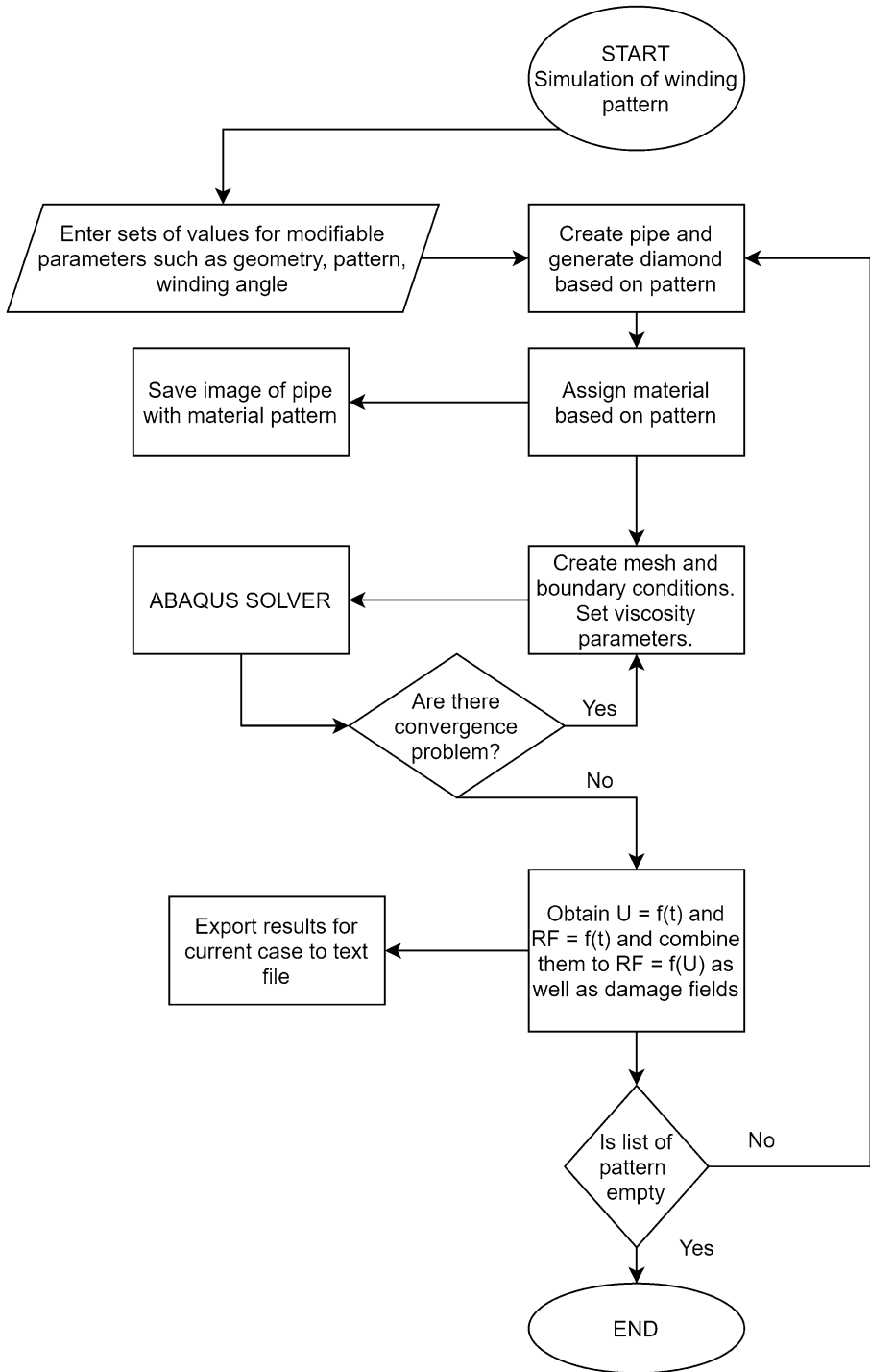

zig - zag area   triangle simplification
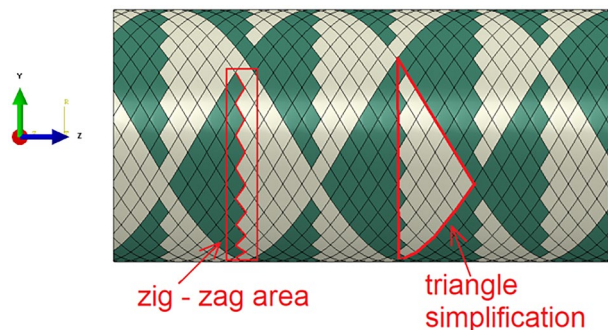
Fig. 4 Workflow of python script created to evaluate the impact of a different pattern on winding pipes strength
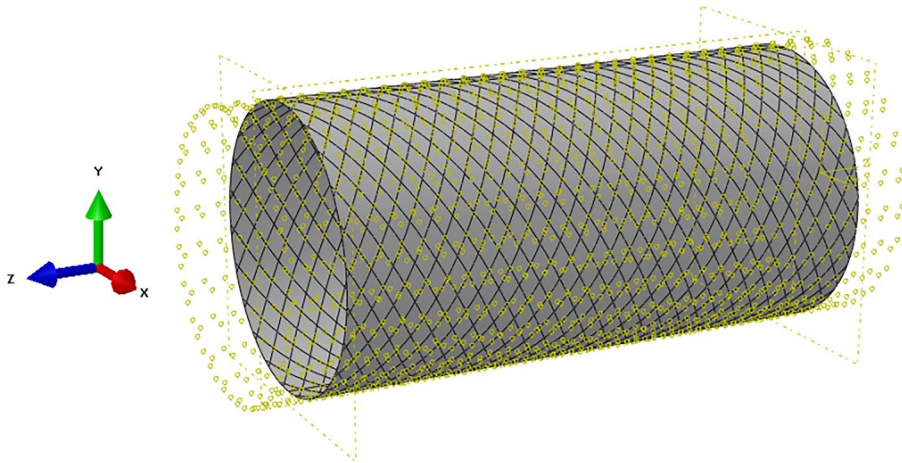
Fig. 5 Representation of bands arrangement on the geometrical model of the tube. Yellow datum points were used to define line projections onto a cylindrical surface

The definition of finite element mesh is affected by previous steps. All datum points that were used to define geometry must be considered as nodes in the final model. This is a reason why a finite element mesh can cause some divergence problem later. Depending on preliminary simulations, quad-dominated or tri mesh elements were chosen. Additionally, element viscosity was regulated between 1e-5 and 1e-3. If divergence in simulation is judged unlikely, a mesh is refined automatically. The script gives a few possibilities of boundary conditions representing different loading cases – internal pressure, radial compression and longitudinal compression. When the numerical model is prepared, the input file is generated. In the next step, the numerical simulations are conducted using Simulia Abaqus Solver [35]. Results are automatically obtained and saved as a text file.

In the current research, the behaviour of composite wound pipes under radial compression loading was investigated. The experimental results as well as the material and geometrical data were derived from the experimental research team (Lisôba et al. [34] and Dalibor et. al. [36]). In Fig. 9 the most important geometric parameters are presented. Some of them can vary between model – especially thickness which in manufactured pipes, depends on the degree of covering. The width of the band is the same for all model (all patterns), but the number of bands differs.
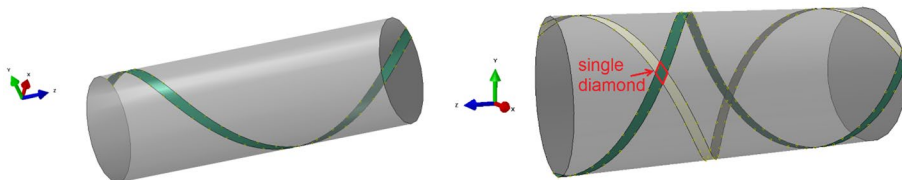

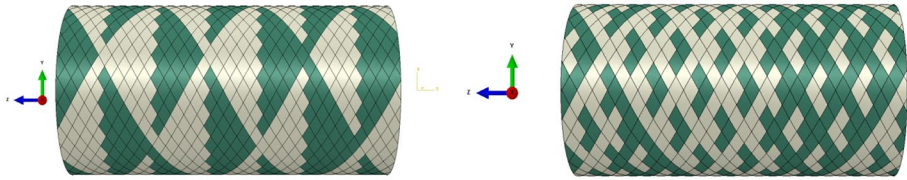**Fig. 6** Half cycle of winding (left) and a single cycle of winding (right)

Fig. 7 Different patterns 2/1 (left) and7/1 (right)

Pipes were manufactured using Toray T700-12 K-50C carbon fibre and UF3369 [34]. As mentioned before, this material was defined as lamina type – 6 needed engineering constants are presented in Table 1. The Hashin criterion to model damage process in pipes was implemented. Data used in the simulation can be found in Table 2. Finally, (Table 3) fracture energy for tension and compression were set based on typical values for this kind of composite materials found in the literature [33, 37].

Wound pipes can be loaded in various ways. Experimental tests reflect real loading conditions. Most popular tests are pressure burst test, radial compression and longitudinal compression. In this paper, radial compression was taken into account. Experimentally it is realized by using two stiff plates which compress the pipe. The tests were performed on and Instron Universal testing machine 3382 in accordance with recommendations of ASTM D2412 by Lisôba et al. [34]. Boundary conditions used in simulations reflect this approach – two rigid body plates are used and the simulation is displacement-driven. In Fig. 10, boundary conditions used in simulations are presented.

Preliminary simulations conducted during the research showed that mesh size has some influence on obtained results. A mesh sensitivity study was realized for a few arbitrary chosen mesh size until convergence is achieved. In Fig. 11, results of this analysis
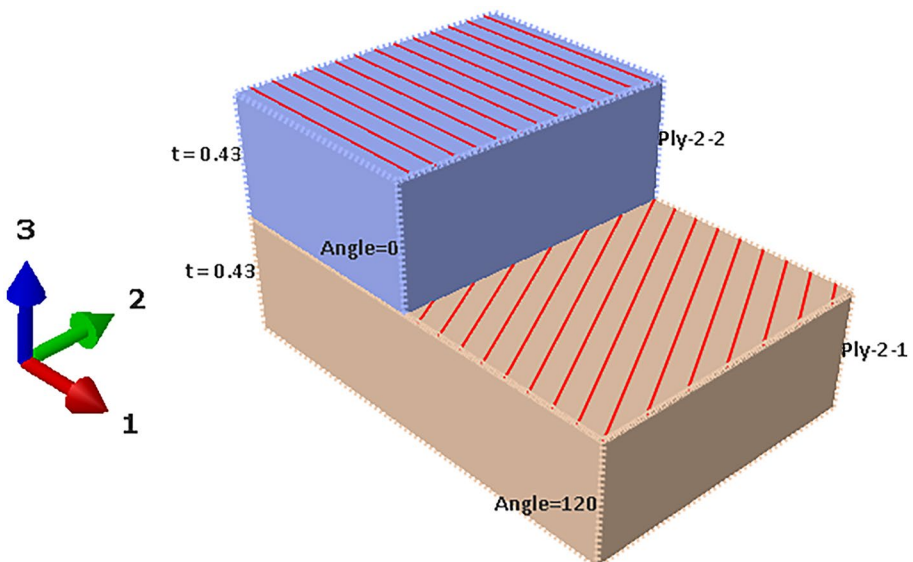

Fig. 8 Ply stack plot of composite (winding angle 60°)
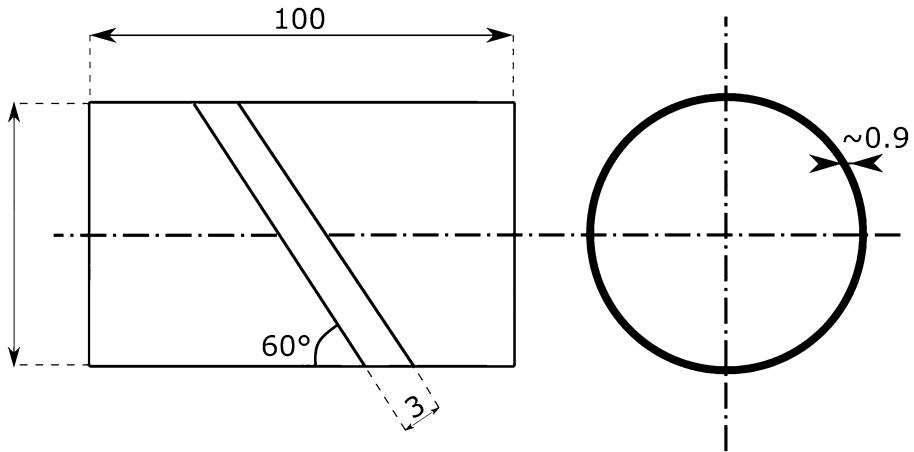
Fig. 9 Important geometric parameters of numerical models

are presented – maximum force and the displacement at the failure were used to found proper mesh size. Based on this analysis, the maximum element size of 2 mm leads to convergence.

Based on presented above preliminary studies mesh size of 1.4 mm was chosen as right choice in term of time-consuming and reliability. Quadratic quadrilateral elements of type S8R as well as quadratic triangular elements of type STRI65 were used to create the discrete model of the pipe. In case of plates (which were modelled as a rigid body) linear quadrilateral elements of type R3D4 were used.

4 Results and Discussion

Based on the presented geometrical and material data simulations of pipes with patterns from 1/1 to 7/1 were conducted. The python script was used to create geometry and numerical model. Next, Abaqus solver was used to simulate the radial compression. In Fig. 12, force–displacement curve is presented for pattern 1/1 (with the lowest number of interlaces). Curve obtained from simulation (red colour) is presented along with experimental results from Lisbôa et al. [34] to enable comparisons.

In Fig. 13 results for the rest of patterns (from 2/1 to 7/1) are presented (red curves) along with experimental data [34].

Pattern 1/1 (Fig. 12, Fig. 13): The elastic part of the curve reflects almost ideally the experiment. Due to the lack of delamination and more smooth stiffness degradation, there

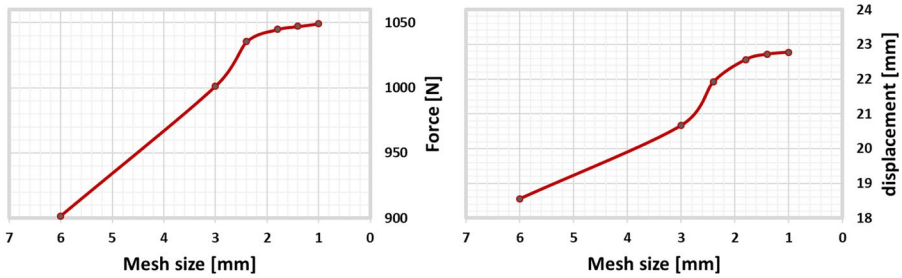**Fig. 10** Boundary conditions radial compression
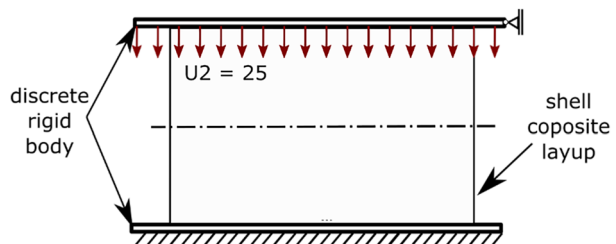
Fig. 11 Mesh sensitivity analysis breaking force as a function of mesh size (left) and breaking displacement as a function of mesh size (right)

is no "sawtooth" effect. In the experiment, the significant drop in the loading force was caused by substantial delamination. Therefore, the simulation did not indicate these drop and the force increased until Hashin failure criteria were satisfied, which happened around 18 mm of displacement. However, even without "sawtooth" effect, the damage was gradually indicated in the simulation, which led to similar value of maximum force.

Pattern 2/1 and 3/1 (Fig. 13a, Fig. 13b): The experiment and simulation showed almost linear behavior up to 8 mm. For 2/1 pattern the damage presented also the "sawtooth" effect, both before and after the point of the maximum force. In the case of 3/1, a more smooth degradation was observed. The numerical analyses followed the experimental curves, however, without the sudden drops of the reaction force. Instead, a typical for these kind of composite materials simulation with Hashin failure criteria gradual damage was obtained.

Pattern 4/1 and 6/1 (Fig. 13c, Fig. 13e): Similar to patterns 2/1 and 3/1 in both experiment and simulation the stiffness of tube was gradually decreased. However, in the case of 4/1 a few experimental specimens presented a higher maximum force, but with dramatic drop of the stiffness. The rest started with a gradual damage, similar to the behavior in the simulation and to the specimens for 2/1 and 3/1 patterns. For 6/1 the discrepancy in

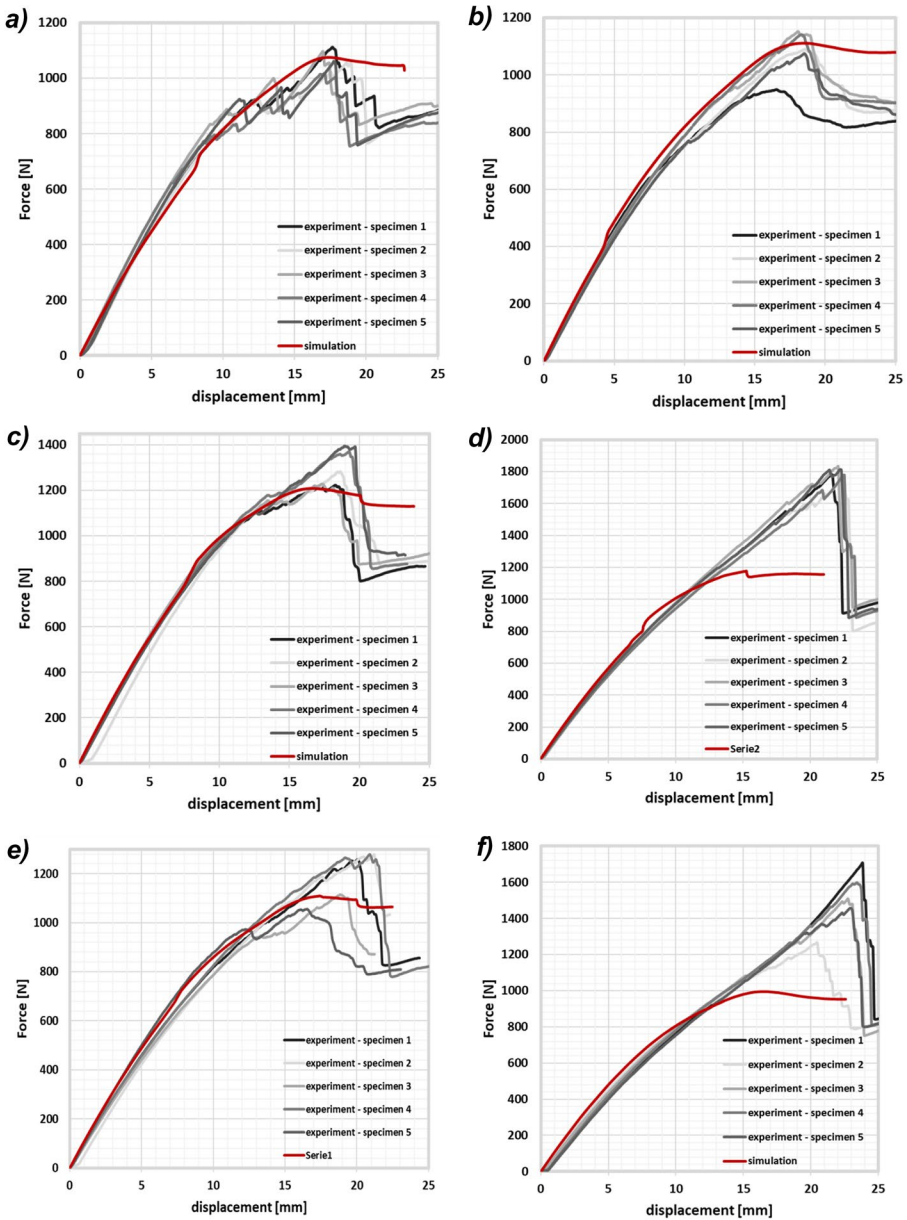**Fig. 12** Force–displacement curve for pipe with 1/1 pattern
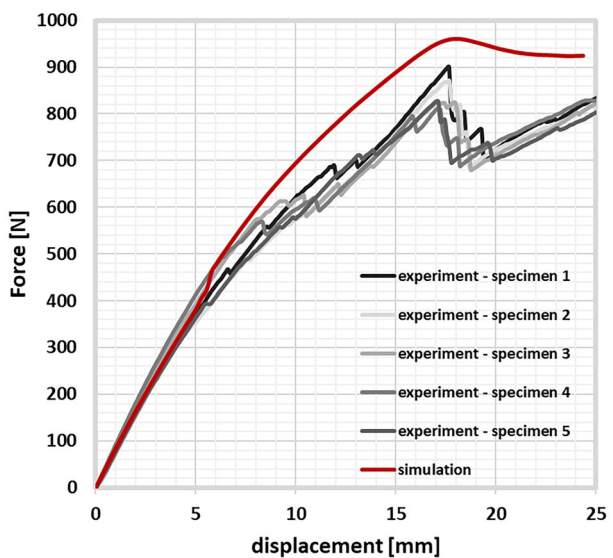
Fig. 13 Force displacement curves from compression of pipes with patterns from 2/1 to 7/1

experimental occurred in the same way, but with longer gradual damage before a dramatic drop in the reaction force. The simulation, however, fits between the experimental variance.

Pattern 5/1 and 7/1 (Fig. 13d, Fig. 13f) No both cases the specimens exhibit the highest maximum forces with almost linear behavior up to the fracture and dramatic drop of load-carrying. These effect is probably caused by significantly higher degree of coverage
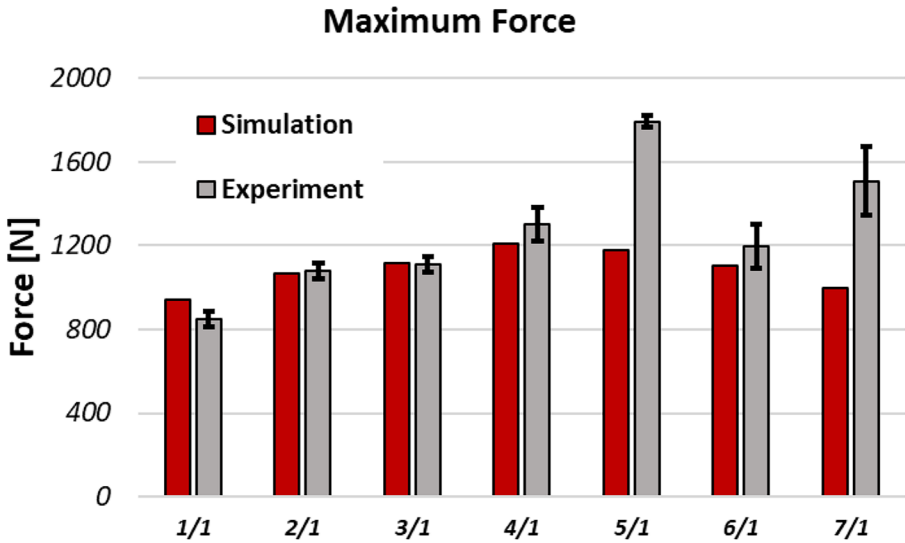
Maximum Force

Fig. 14 Comparison of maximum forces in experiment and simulation regarding a specific pattern (n/1)

in these two cases (112.5% and 120.2%) in comparison to i.e. pattern 2/1 or 3/1 with 104%. The excessive volume of the composite causes that the neighboring yarns overlap each other. Therefore, this additional inter weavings might act as a physical barrier for the damage of the composite.

The summary comparison of the two specific values of the experiment, maximum force and displacement at the maximum force, is shown in Fig. 14 and Fig. 15. In general, a very satisfactory agreement was found in the cases of patterns 1/1, 2/1, 3/1, 4/1 and 6/1, both
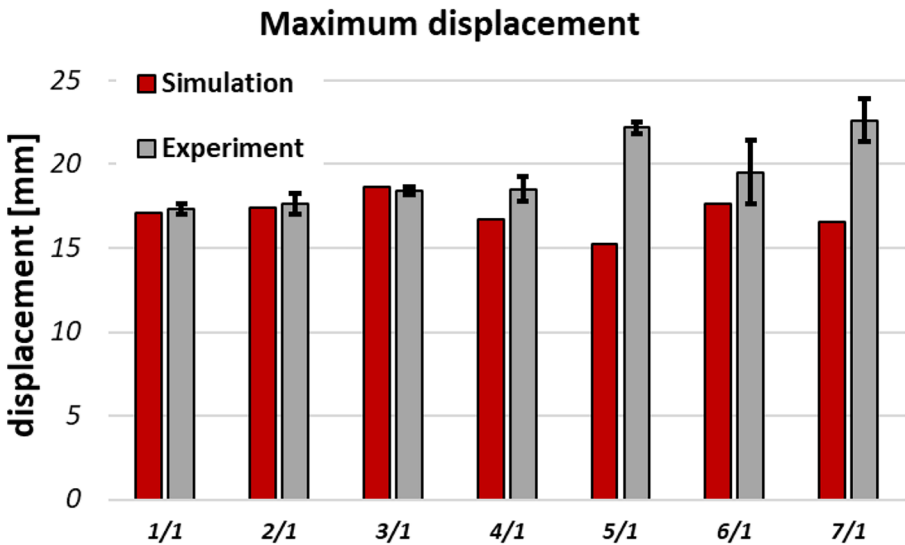
Maximum displacement

Fig. 15 Comparison of the displacement at which failure occurred in experiment and simulation regarding a specific pattern (n/1)
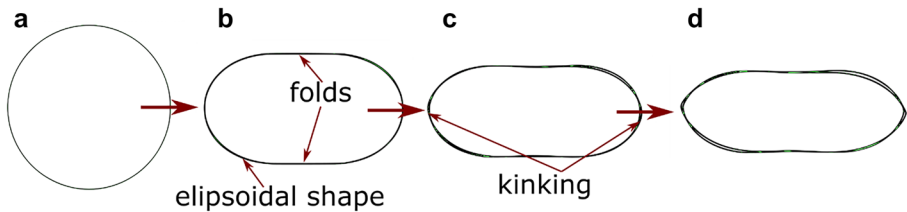
Fig. 16 Change of geometry during compression test pipe with pattern 3/1. **a**) pipe before compression **b**) during damage process forming of folds **c**) geometry when rapture damage occurs with kinking of fibres **d**) geometry after 25 mm of compressions

in maximum force and the displacement at that force. However, as mentioned above, the experimental maximum forces in patters 5/1 and 7/1 exceeded the numerical ones because of values of degree of coverage.(See. Fig. 19)

Independently from the pattern, it is possible to point characteristic changes in pipe geometry. The pipes have a circular section at the beginning (Fig. 16a), but during the compression their shape becomes more elliptical. Small folds show up at the outer part of contact between pipe surface and plates (Fig. 16b). At the moment of rupture decrease in force, kinking of fibres is observable (Fig. 16c). More kinking and growth of pockets are present in the final phase.

In Fig. 17 the change of radial deflection (in a cylindrical coordinate system) for pipe with pattern 3/1 after 25 mm of compression is shown. The change of the shape was similar for other patterns (cf. Fig. 16d).

Fibre compression is a dominant reason for damage in the last phase of the test. It occurs in the place when kinking is observable (cf. Fig. 16c, d). This is the place where compressive stresses have maximum values. Field of stresses in fibre direction is presented in Fig. 18. It is worth to notice that the zig-zag area affect the stress field. The line of maximum damage is also affected by this as it is shown in Fig. 20.

In Fig. 19 different phases of the damage behaviour of fiber compression are shown. First damage occurs in the triangle area, on the borders of the laminate area. Then, the damage is observed in the "zig-zag" area.
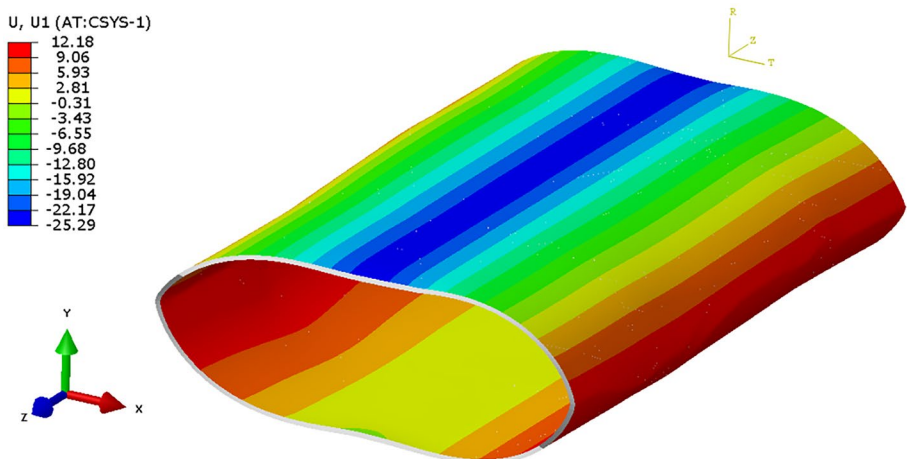

Fig. 17 Change of radial deflection (pipe with pattern 3/1 after 25 mm of compression)
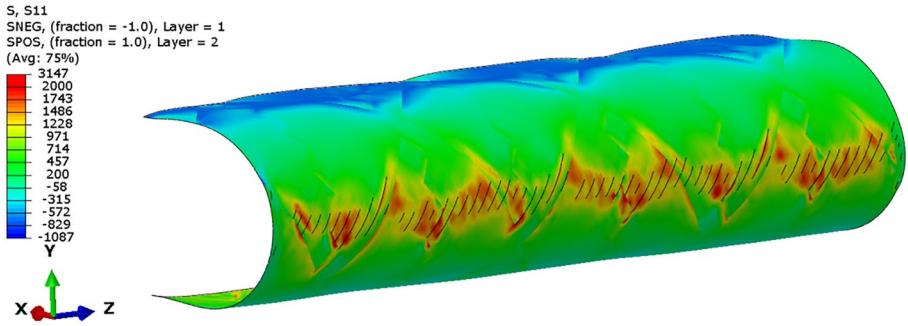
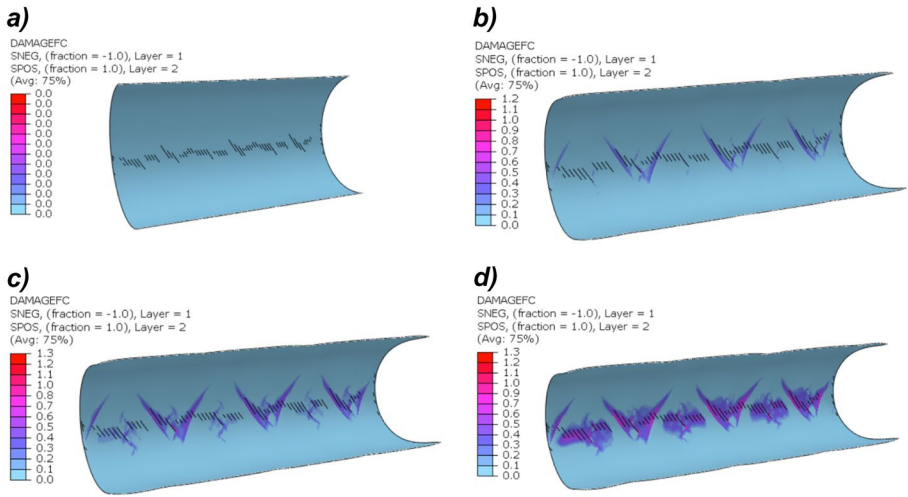**Fig. 18** Stress field in the fiber direction

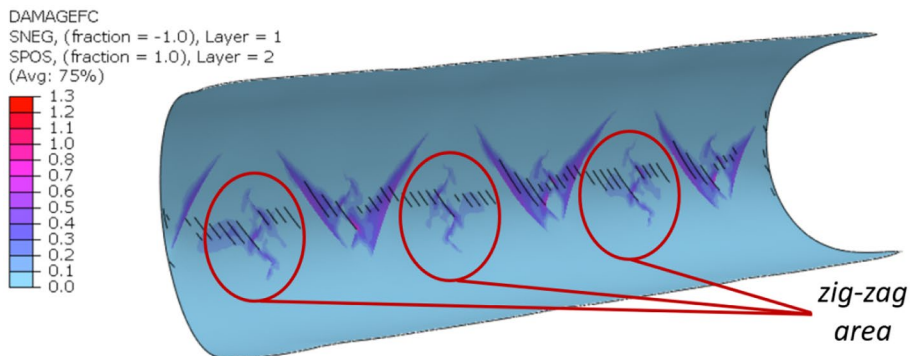**Fig. 19** Fiber compression damage fields in different displacement steps: 0 mm (**a**), 15 mm (**b**), 17.5 mm (**c**), 20 mm (**d**)

Fig. 20 Fiber compression damage just before the maximum force

Table 1 - Elastic properties of composite

$E_1[MPa]$	$E_2[MPa]$	$v[-]$	$G_{12}[MPa]$	$G_{13}[MPa]$	$G_{23}[MPa]$
153000	12200	0.34	5900	5900	2100

Table 2 - Strengths of material in a longitudinal, transverse direction and in-plane shear strength

$X_t[MPa]$	$X_c[MPa]$	$Y_t[MPa]$	$Y_c[MPa]$	$S_{12}[MPa]$	$S_{21}[MPa]$
1822	890	69.9	153	75.7	70

Table 3 - Fracture energy in tension (t) and compression (c) for longitudinal (1) and transverse (2) direction

$G_{1t}\left[\frac{N}{mm}\right]$	$G_{1c}\left[\frac{N}{mm}\right]$	$G_{2t}\left[\frac{N}{mm}\right]$	$G_{2c}\left[\frac{N}{mm}\right]$
89.8	78.3	0.8	0.8

Figure 20 presents in detail the "zig-zag" area for the tube with 3/1 pattern.

The rest of damage modes for 3/1 patterns are presented for the displacement of 18 mm (at the maximum force) in Fig. 21. It is noticeable, that the damage in matrix plays also a significant role. Nevertheless, damage fields are more smooth and uniform, without such a big influence of the pattern geometry.

To sum up, the analysis of numerical simulations carried out for different patterns as well as available experimental data shows that the mechanism of damage in compressed filament-wound tubes are based on several stages. Firstly, damage of matrix
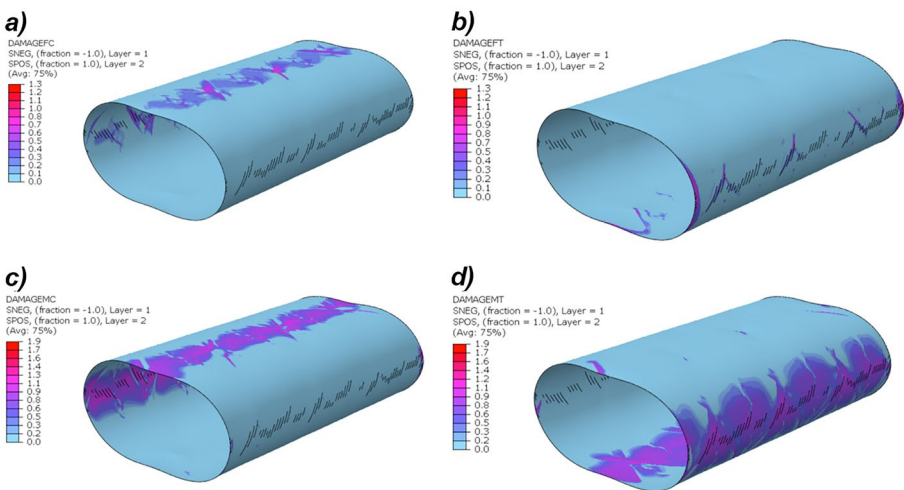

Fig. 21 Damage fields in pattern 3/1 at the displacement of 18 mm (at maximum force) for fiber compression (**a**), fiber tension (**b**), matrix compression (**c**) and matrix tension (**d**)

causes gradual lowering of stiffness. It can be observed in the force–displacement curves as a deviation from linear characteristic after first several millimeters. Then in the next stage – the final damage occurs when fibers start to kink as an effect of compression in the side areas. These behavior is also observed in both simulation and experimental data. However, in the case of tubes with high level of coverage degree i.e. 7/1 pattern with the covering over 120%, there is additional stiffening effect. This effect causes fast grow of force and then rupture breaking.

5 Conclusions

A numerical study of the filament-wound pipes under radial compression was conducted. A finite element model was developed to reflect the material distribution with respect to the winding pattern. In order to implement the progressive damage Hashin model was used. The numerical simulations were compared with the experimental data obtained by Lisbôa et al. [34].

The following conclusions were established:

- The simulations reflected the experiment with a good agreement. The implemented the "zig-zag" area influences the stress distribution resulting in a less homogeneous stress field. Especially, regarding the fiber tension and compression damage modes.
- The main cause of the damage during simulations is fiber compression in the side area analogical to experimental tests. The first signs of this process were found in triangles and the "zig-zag" areas similar to real tests. This observation proves that the "zig-zag" zone should be taken into consideration during numerical simulations.
- The higher value of thickness reflects the degree of covering in the simulation. Nevertheless, this is not the only effect. In a real filament-wound pipe, the additional "portion" of the composite is performed as an overlap of the neighboring bands. This overlap, indeed, results in an additional number of interweavings and rise in general stiffness in the elastic part of load–displacement curve. Therefore, the impact of pattern number should be analyzed with the degree of covering as close to 100% as possible.
- The implemented Hashin criteria reflected the failure of the pipes with a good prediction especially in the case of lower degree of coverage. Nevertheless, since the delamination failure mode is not considered, the characteristic drops in experimental results could not be achieved in the simulation.
- The cases with higher degree of freedom exhibited a dramatic, rapture loose of stiffness after the maximum force obtained. These occurred in tubes with pattern 5/1, 7/1 and partially in 4/1. It indicates, that even if there is a significant gain in the maximum force, a less predictable and safe failure occurs.
- Taking into consideration the practical aspect of the investigation, one may find it beneficial to more properly simulate the behavior of filament-wound pipes so as to shorten an expensive and time-consuming experimental campaign.

References

1. Wang, R., Jiao, W., Liu, W., Yang, F.: A new method for predicting dome thickness of composite pressure vessels. J. Reinf. Plast. Compos. **29**, 3345–3352 (2010). https://doi.org/10.1177/0731684410376330
2. Zu, L., Koussios, S., Beukers, A.: A novel design solution for improving the performance of composite toroidal hydrogen storage tanks. Int. J. Hydrogen Energy. **37**, 14343–14350 (2012). https://doi.org/10.1016/j.ijhydene.2012.07.009
3. Rafiee, R., Torabi, M.A.: Stochastic prediction of burst pressure in composite pressure vessels. Compos. Struct. **185**, 573–583 (2018). https://doi.org/10.1016/j.compstruct.2017.11.068
4. Vasiliev, V. V., Morozov, E. V.: Advanced Mechanics of Composite Materials and Structural Elements. Elsevier Ltd (2018)
5. Xia, M., Takayanagi, H., Kemmochi, K.: Analysis of multi-layered filament-wound composite pipes under internal pressure. Compos. Struct. **53**, 483–491 (2001). https://doi.org/10.1016/S0263-8223(01)00061-7
6. Soden, P.D., Leadbetter, D., Griggs, P.R., Eckold, G.C.: The strength of a filament wound composite under biaxial loading. Composites. **9**, 247–250 (1978). https://doi.org/10.1016/0010-4361(78)90177-5
7. Bai, J., Seeleuthner, P., Bompard, P.: Mechanical behaviour of ±55° filament-wound glass-fibre/epoxy-resin tubes: I. Microstructural analyses, mechanical behaviour and damage mechanisms of composite tubes under pure tensile loading, pure internal pressure, and combined loading. Compos. Sci. Technol. 57, 141–153 (1997). https://doi.org/10.1016/S0266-3538(96)00124-8
8. Mian, H.H., Wang, G., Dar, U.A., Zhang, W.: Optimization of composite material system and lay-up to achieve minimum weight pressure vessel. Appl. Compos. Mater. **20**, 873–889 (2013). https://doi.org/10.1007/s10443-012-9305-4
9. Hernández-Moreno, H., Douchin, B., Collombet, F., Choqueuse, D., Davies, P.: Influence of winding pattern on the mechanical behavior of filament wound composite cylinders under external pressure. Compos. Sci. Technol. **68**, 1015–1024 (2008). https://doi.org/10.1016/j.compscitech.2007.07.020
10. Almeida, J.H.S., Ribeiro, M.L., Tita, V., Amico, S.C.: Damage and failure in carbon/epoxy filament wound composite tubes under external pressure: Experimental and numerical approaches. Mater. Des. **96**, 431–438 (2016). https://doi.org/10.1016/j.matdes.2016.02.054
11. Shen, C., Han, X.: Damage and failure analysis of filament wound composite structure considering fibre crossover and undulation. Adv. Compos. Lett. **27**, 55–70 (2018). https://doi.org/10.1177/096369351802700202
12. Manoj Prabhakar, M., Rajini, N., Ayrilmis, N., Mayandi, K., Siengchin, S., Senthilkumar, K., Karthikeyan, S., Ismail, S.O.: An overview of burst, buckling, durability and corrosion analysis of lightweight FRP composite pipes and their applicability. Compos. Struct. 230, (2019). https://doi.org/10.1016/j.compstruct.2019.111419
13. Almeida Júnior, J.H., Ribeiro, M.L., Tita, V., Amico, S.C.: Damage modeling for carbon fiber/epoxy filament wound composite tubes under radial compression. Compos. Struct. **160**, 204–210 (2017a). https://doi.org/10.1016/j.compstruct.2016.10.036
14. Mansour, G., Tzikas, K., Tzetzis, D., Korlos, A., Sagris, D., David, K.: Experimental and Numerical Investigation on the Torsional Behaviour of Filament Winding-Manufactured Composite Tubes. Appl. Mech. Mater. **834**, 173–178 (2016). https://doi.org/10.4028/www.scientific.net/amm.834.173
15. Hu, Y., Yang, M., Zhang, J., Song, C., Zhang, W.: Research on torsional capacity of composite drive shaft under clockwise and counter-clockwise torque. Adv. Mech. Eng. **7**, 1–7 (2015). https://doi.org/10.1177/1687814015582109
16. Diniz Melo, J.D., Levy Neto, F., De Araujo Barros, G., De Almeida Mesquita, F.N.: Mechanical behavior of GRP pressure pipes with addition of quartz sand filler. J. Compos. Mater. **45**, 717–726 (2011). https://doi.org/10.1177/0021998310385593
17. Martins, L.A.L., Bastian, F.L., Netto, T.A.: Reviewing some design issues for filament wound composite tubes. Mater. Des. **55**, 242–249 (2014). https://doi.org/10.1016/j.matdes.2013.09.059
18. Robert, M., Fam, A.: Long-term performance of GFRP tubes filled with concrete and subjected to salt solution. J. Compos. Constr. **16**, 217–224 (2012). https://doi.org/10.1061/(ASCE)CC.1943-5614.0000251
19. Son, J.K., Fam, A.: Finite element modeling of hollow and concrete-filled fiber composite tubes in flexure: Model development, verification and investigation of tube parameters. Eng. Struct. **30**, 2656–2666 (2008). https://doi.org/10.1016/j.engstruct.2008.02.014
20. Qasrawi, Y., Heffernan, P.J., Fam, A.: Dynamic behaviour of concrete filled FRP tubes subjected to impact loading. Eng. Struct. **100**, 212–225 (2015a). https://doi.org/10.1016/j.engstruct.2015.06.012
21. Qasrawi, Y., Heffernan, P.J., Fam, A.: Performance of concrete-filled FRP tubes under field close-in blast loading. J. Compos. Constr. **19**, 1–12 (2015b). https://doi.org/10.1061/(ASCE)CC.1943-5614.0000502

22. Eggers, F., Almeida, J.H.S., Azevedo, C.B., Amico, S.C.: Mechanical response of filament wound composite rings under tension and compression. Polym. Test. **78**, (2019). https://doi.org/10.1016/j.polymertesting.2019.105951

23. Zu, L., Xu, H., Wang, H., Zhang, B., Zi, B.: Design and analysis of filament-wound composite pressure vessels based on non-geodesic winding. Compos. Struct. **207**, 41–52 (2019). https://doi.org/10.1016/J.COMPSTRUCT.2018.09.007

24. Almeida Júnior, J.H., Ribeiro, M.L., Tita, V., Amico, S.C.: Stacking sequence optimization in composite tubes under internal pressure based on genetic algorithm accounting for progressive damage. Compos. Struct. **178**, 20–26 (2017b). https://doi.org/10.1016/j.compstruct.2017.07.054

25. Rousseau, J., Perreux, D., Verdière, N.: The infuence of winding patterns on the damage behaviour of flament-wound pipes. Compos. Sci. Technol. **59**, 1439–1449 (1999). https://doi.org/10.1016/S0168-583X(00)00540-1

26. Morozov, E.V.: The effect of filament-winding mosaic patterns on the strength of thin-walled composite shells. Compos. Struct. **76**, 123–129 (2006). https://doi.org/10.1016/j.compstruct.2006.06.018

27. Azevedo, C.B., Humberto, J., Almeida, S., Flores, H.F., Eggers, F., Amico, S.C.: Influence of mosaic pattern on hygrothermally-aged filament wound composite cylinders under axial compression. J. Compos. Mater. **54**, 2651–2659 (2020). https://doi.org/10.1177/0021998319899144

28. Shen, C., Han, X., Guo, Z.: A new method for calculating the stiffness of filament wound composites considering the fibre undulation and crossover. Adv. Compos. Lett. **23**, 88–95 (2014). https://doi.org/10.1177/096369351402300402

29. Błażejewski, W.: Kompozytowe zbiorniki wysokociśnieniowe wzmocnione włóknami według wzorów mozaikowych. Oficyna Wydawnicza Politechniki Wrocławskiej (2013)

30. Hashin, Z.: Failure Criteria for Unidirectional Fiber Composites. J. Appl. Mech. **47**, 329–334 (1980). https://doi.org/10.1115/1.3153664

31. Hashin, Z., Rotem, A.: A Fatigue Failure Criterion for Fiber Reinforced Materials. J. Compos. Mater. **7**, 448–464 (1973). https://doi.org/10.1177/002199837300700404

32. Barbero, E.J., Cosso, F.A., Roman, R., Weadon, T.L.: Determination of material parameters for Abaqus progressive damage analysis of E-glass epoxy laminates. Compos. Part B Eng. **46**, 211–220 (2013). https://doi.org/10.1016/j.compositesb.2012.09.069

33. Lapczyk, I., Hurtado, J.A.: Progressive damage modeling in fiber-reinforced materials. Compos. Part A Appl. Sci. Manuf. **38**, 2333–2341 (2007). https://doi.org/10.1016/j.compositesa.2007.01.017

34. Lisbôa, T.V., Almeida, J.H.S., Dalibor, I.H., Spickenheuer, A., Marczak, R.J., Amico, S.C.: The role of winding pattern on filament wound composite cylinders under radial compression. Polym. Compos. **41**, 2446–2454 (2020). https://doi.org/10.1002/pc.25548

35. Abaqus 6.14, Analysis User's Manual, Dassault System, (2014)

36. Dalibor, I.H., Lisbôa, T.V., Marczak, R.J., Amico, S.C.: Optimum slippage dependent, non-geodesic fiber path determination for a filament wound composite nozzle. Eur. J. Mech. A/Solids. **82**, 103994 (2020). https://doi.org/10.1016/j.euromechsol.2020.103994

37. Girão Coelho, A.M., Toby Mottram, J., Harries, K.A.: Finite element guidelines for simulation of fibre-tension dominated failures in composite materials validated by case studies. Compos. Struct. **126**, 299–313 (2015). https://doi.org/10.1016/j.compstruct.2015.02.071

Springer